

# Detection of decoupled surface and bulk states in epitaxial orthorhombic SrIrO<sub>3</sub> thin films

Prescott E. Evans,<sup>a</sup> Takashi Komesu,<sup>a</sup> Le Zhang,<sup>a</sup> Ding-Fu Shao,<sup>a</sup> Andrew J. Yost,<sup>a</sup> Shiv Kumar,<sup>b</sup> Eike F. Schwier,<sup>b</sup> Kenya Shimada,<sup>b</sup> Evgeny Tsybal,<sup>a</sup> Xia Hong,<sup>a</sup> and P. A. Dowben<sup>a</sup>

<sup>a</sup>Department of Physics and Astronomy & Nebraska Center for Materials and Nanoscience, Theodore Jorgensen Hall, 855 N 16th, University of Nebraska, 880299, Lincoln, NE 68588-0299, U.S.A.

<sup>b</sup>Hiroshima Synchrotron Radiation Center, Hiroshima University, Higashi-Hiroshima 739-0046, Japan

## Abstract:

We report the experimental evidence of evolving lattice distortion in high quality epitaxial orthorhombic SrIrO<sub>3</sub>(001) thin films fully strained on (001) SrTiO<sub>3</sub> substrates. While the surface layer of 5 nm SrIrO<sub>3</sub> films is Sr-O terminated, subsequent layers recover the semi-metallic state, with the band structure consistent with an orthorhombic SrIrO<sub>3</sub>(001) having the lattice constant of the substrate. While there is no band folding in the experimental band structure, additional super-periodicity is evident in low energy electron diffraction measurements, suggesting the emergence of a transition layer with crystal symmetry evolving from the SrTiO<sub>3</sub> substrate to the SrIrO<sub>3</sub>(001) surface. Our study sheds light on the misfit relaxation mechanism in epitaxial SrIrO<sub>3</sub> thin films in the orthorhombic phase, which is metastable in bulk.

**Keywords:** Iridate thin films, Angle Resolved Photoemission Spectroscopy, electronic structure, surface termination, strain relaxation.

corresponding author's email address: pdowben1@unl.edu

## I. Introduction

The combination of strong spin-orbit interactions and electron correlation has driven the recent research interest in 5d irridates,<sup>1-6</sup> including the correlated semimetal SrIrO<sub>3</sub>.<sup>7-12</sup> Orthorhombic SrIrO<sub>3</sub>, as schematically shown in Figure 1a-b, has been theoretically predicted to host non-trivial topological phases.<sup>10</sup> While the crystal structure of bulk SrIrO<sub>3</sub> favors the monoclinic distortion of the hexagonal BaTiO<sub>3</sub> structure<sup>6,13</sup> rather than the perovskite phase, high-quality orthorhombic SrIrO<sub>3</sub>(001) films have been grown on SrTiO<sub>3</sub>(001),<sup>7,9,14</sup> (LaAlO<sub>3</sub>)<sub>0.3</sub>(SrAl<sub>1/2</sub>Ta<sub>1/2</sub>O<sub>3</sub>)<sub>0.7</sub><sup>8,14</sup> and GdScO<sub>3</sub><sup>12</sup> substrates. Epitaxial SrIrO<sub>3</sub> films in the ultrathin limit exhibit a range of interesting properties, including dimensionality crossover, metal-insulator transition and enhanced spin relaxation time,<sup>9,11,15</sup> and it is essential to understand how the electronic structure and lattice distortion evolve in these thin films.

The goal of this research is to further examine the crystal symmetry in epitaxial orthorhombic SrIrO<sub>3</sub> thin films. This is key to any effort to exploit the interfacial charge and control quantum confinement to engineer the electronic and magnetic states in SrIrO<sub>3</sub>. Furthermore, characterizing the thin film is also important to gain a deeper understanding of the finite size effects<sup>9,11,15</sup> for SrIrO<sub>3</sub> in this metastable phase.<sup>10</sup> Previous studies have shown that epitaxial SrIrO<sub>3</sub> films strained on SrTiO<sub>3</sub>(001) are insulating when the films were thinner than 4 unit cells thick.<sup>9,11,15</sup> Obviously, thinner SrIrO<sub>3</sub>(001) films are much more dominated by the surface. A key question is how the effect of epitaxial strain is entangled with the quantum confinement, in determining the electronic properties of these ultrathin films.

## II. Experimental and Theoretical Methods

The SrIrO<sub>3</sub> thin films were grown on Ti-O terminated (001) SrTiO<sub>3</sub> and Nb doped SrTiO<sub>3</sub> (Nb:SrTiO<sub>3</sub>; 0.05 wt%) substrates using off-axis radio frequency magnetron sputtering. The films were deposited at 600 °C in 150 mTorr process gas, composed of Ar and O<sub>2</sub> (ratio 2:1). The detailed growth conditions can be found elsewhere.<sup>15</sup> We performed the surface morphology and structure characterizations on SrIrO<sub>3</sub>(001) samples grown on SrTiO<sub>3</sub> substrates. The spectroscopic measurements were performed on SrIrO<sub>3</sub>(001) grown on Nb:SrTiO<sub>3</sub>. After retrieving the samples from the growth chamber, the films were promptly sealed in vacuum to minimize the exposure to ambient condition prior to the spectroscopy investigations. Four separate 5 nm samples were studied, and the results were consistent from sample to sample.

The surface morphology was examined using a Bruker Multimode8 atomic force microscopy (AFM) under the tapping mode. Figure 2a shows an AFM topography image of a 5 nm SrIrO<sub>3</sub>(001) film, which exhibits atomically smooth terraces separated by 4 Å steps. The typical root mean square (RMS) roughness is 2 Å. The structure characterizations were performed using the Rigaku SmartLab X-ray diffractometer (XRD), with a copper source ( $\lambda_{K\alpha} = 1.5406$  Å). Figure 2c shows the out-of-plane XRD measurement on the same sample as in Fig. 2a. The as-grown SrIrO<sub>3</sub> film is single crystalline with no impurity phases, and the deduced *c*-axis lattice constant is ~4.02 Å, which is consistent with the compressive strain imposed by the SrTiO<sub>3</sub>(001) substrate (-1.14 %). The typical rocking curves for the 5 nm films have the full-width-half-maximum less than 0.1°, attesting to the high crystalline quality of the samples. The film thickness was extracted by fitting to the finite-size oscillations around main Bragg peaks (Fig. 2c inset) and the X-ray reflectivity (XRR) measurement (Fig. 2d). In a previous study,<sup>14</sup> using the reciprocal space mapping (RSM) and pole figure techniques, we have shown that the SrIrO<sub>3</sub> films are fully strained (up to 21 nm) and conform to the four-fold symmetry of SrTiO<sub>3</sub>, indicating the films are in the orthorhombic phase.

The experimental electronic structure measurements were performed on 5 nm thick SrIrO<sub>3</sub> films using several spectroscopic methods. The high-resolution angle-resolved photoemission spectroscopy (HR-ARPES) measurements were performed on the linear undulator beamline (BL-1) of the Hiroshima Synchrotron Radiation Center (HiSOR), Hiroshima University.<sup>16,17</sup> We have measured HR-ARPES using a photon energy of 150 eV in the p-polarization geometry, where the electric field vector lies in the plane of incidence as well as the photoelectron detection plane. Based on the matrix elements of the dipole transition, one can mainly detect the initial-state orbitals having even symmetry with respect to the mirror plane, which coincides with the plane of incidence. The surface stoichiometry of SrIrO<sub>3</sub>(001) was established by angle-resolved X-ray photoemission spectroscopy (ARXPS), obtained using non-monochromatized Al K $\alpha$  x-ray source, with photon energy of 1486.6 eV, and a SPECS PHOIBOS 150 energy analyzer. The emission angles for ARXPS are all with respect to the surface normal. Several successive annealing steps at  $\sim 150^\circ\text{C}$  changes the surface stoichiometry only slightly. Low energy electron diffraction (LEED) patterns confirming surface lattice were taken *in situ* using an Omicron SPECTALEED rear-view LEED optics system with an electron beam energy of 31.5 eV, and was seen to be very sensitive to surface preparation. The experimental band structure was compared with first-principles density functional theory (DFT) calculations, which were performed using a plane-wave pseudopotential method with fully-relativistic ultrasoft pseudopotentials,<sup>18</sup> as implemented in Quantum-ESPRESSO.<sup>19</sup> The exchange and correlation effects were treated within the generalized gradient approximation (GGA).<sup>20</sup> In the calculation, we used the plane-wave cut-off energy of 60 Ry, and a  $16 \times 16 \times 16$  k-point mesh in the irreducible Brillouin zone. We used a  $\sqrt{2}a_0 \times 2a_0 \times \sqrt{2}a_0$  orthorhombic unit cell in the calculation, with  $a_0 = a_{\text{STO}} = 3.905 \text{ \AA}$ . All the atomic coordinates were relaxed until the force on each atom was less than  $0.001 \text{ eV/\AA}$ . Spin-orbit coupling was included in all electronic structure calculations. The calculated band structure is unfolded into the Brillouin zone for SrIrO<sub>3</sub> without distortion (Figure 1a) using the code BandUP.<sup>21,22</sup>

### III. Surface Termination

From the x-ray photoemission spectra, we find that the topmost Sr-O surface layer is distinct from the bulk. Confirmation that the surface termination of SrIrO<sub>3</sub>(001) is Sr-O comes from plotting the Sr to Ir core level intensity as a function of emission angle. In Figure 3b, the Sr 3d to the Ir 4f core level photoemission intensities have been plotted, as a function of emission angle. This ratio increases at the very highest take-off angles, which in turn are the most surface sensitive.<sup>23-25</sup> For a conductive oxide like SrIrO<sub>3</sub>, the electron mean free path varies from about 15  $\text{\AA}$  at  $0^\circ$  to about 2.6  $\text{\AA}$  at  $80^\circ$  incident angle for an electron kinetic energy of about 1300 eV, because as this system is metallic there are plasmon electron kinetic energy loss mechanisms. Since the larger takeoff angles are highly surface sensitive, this tends to suggest that the surface is Sr-O terminated and suggests there is a large difference in enthalpy between the surface and the bulk.

Several successive sample annealing treatments, at  $\sim 150^\circ\text{C}$ , changes the surface stoichiometry only slightly, as is evident in the Sr 3d to the Ir 4f core level photoemission intensities. This is in spite of the fact that annealing the surface successively leads to elimination of the expected C<sub>4v</sub> LEED pattern, possibly as a result of IrO<sub>2</sub> sublimation.<sup>9,26</sup> The very sharp increase in the relative Sr 3d intensity and increase in core level binding energy suggests that the surface electronic structure, due to the Sr-O termination, is extremely thin and restricted to the topmost surface. This Sr-O surface termination, observed here, is consistent with prior growth studies where a 'self-organized' conversion of the surface termination IrO<sub>2</sub> to SrO during the initial growth of SrIrO<sub>3</sub><sup>9</sup> and from RuO<sub>2</sub> to Sr-O in the growth of SrRuO<sub>3</sub>.<sup>26</sup>

Recent transport studies have shown that the critical thickness for a metal-insulator transition is 4 unit cell in bare  $\text{SrIrO}_3$  thin films<sup>15</sup> and 3 unit cell in  $\text{SrIrO}_3$  films encapsulated by  $\text{SrTiO}_3$  top layers,<sup>11</sup> which clearly illustrate the potential influence of the surface layer at the atomic scale. In this regard,  $\text{SrIrO}_3$  differs significantly from other oxides, like strontium perovskites,<sup>27</sup> where the Sr enrichment at the surface persists well away from the surface. Additionally, unlike many other oxides or perovskites, the surface of  $\text{SrIrO}_3$  is incredibly fragile. Changes in vacuum conditions and modest annealing were seen to lead to a reduction or loss of surface order, as observed in LEED.

In spite of the strong surface to bulk core level shift of Sr, in the Sr-O surface layer, the experimental band structure probed via HR-ARPES is consistent with unreconstructed  $\text{SrIrO}_3(001)$ . Figure 4 shows the band structure of  $\text{SrIrO}_3(001)$  from the  $\bar{\Gamma}$  (surface Brillouin center) to  $\bar{M}$  point (the edge of the surface Brillouin zone). This experimental band structure (Figure 4) is consistent with the semimetallic character of  $\text{SrIrO}_3$ , in excellent agreement with previous reports on orthorhombic  $\text{SrIrO}_3$  thin films<sup>7-9,12</sup>, and very different from the distorted hexagonal  $\text{SrIrO}_3$ .<sup>6</sup> Superimposed on the experimental data along  $-k$  is the DFT calculations of bulk orthorhombic  $\text{SrIrO}_3$ , which well captures the position and energy levels of the heavy and light hole bands. There is clear evidence for an occupied density of states near the measured Fermi level ( $E_F$ ), which is away from the Brillouin center at  $0.7 \text{ \AA}^{-1}$ , as well as significant dispersion of the occupied bands, symmetric about the Brillouin zone edge.<sup>7-9</sup> The Brillouin zone critical  $\bar{M}$  point placement is also consistent with  $a_0 = 3.905 \text{ \AA}$  for  $\text{SrTiO}_3$ . We have increased the energy window of the calculated band structure by a factor of 1.2, to improve the match between theory (left) and experiment (right) in Figure 4. The surface Brillouin zone from the band structure is consistent with the unfolded  $\text{SrIrO}_3(001)$ , i.e. a tetragonal  $\text{SrIrO}_3(001)$ , similar to previous reports.<sup>9</sup>

#### IV. Super-periodicity

Figure 1a shows  $\text{SrIrO}_3$  having the hypothetical perovskite crystal structure without distortion. The black box in Figure 1a denotes the ideal cubic perovskite unit cell. Figure 1b exhibits the real crystal structure of  $\text{SrIrO}_3$  thin film with octahedral distortion.<sup>12</sup> This distortion leads to the orthorhombic unit cell ( $\sqrt{2}a_0 \times 2a_0 \times \sqrt{2}a_0$ ), as shown in Figure 1b. The resulting Brillouin zone is also shown Figure 1c (the small purple volume). In a previous study, Schütz and colleagues<sup>9</sup> found in their LEED studies a  $2 \times 2$  super-periodicity ( $p(2 \times 2)$ ) for 4 unit cell thick films, and a centered  $2 \times 2$  super periodicity (i.e., a  $c(2 \times 2)$  in real space or  $(\sqrt{2}/2) \times (\sqrt{2}/2) \text{ R}45^\circ$  in reciprocal space) for a 3 unit cell thick film. In contrast, the LEED image in Figure 2b shows evidence for a super-periodicity that differs from both of these two aforementioned super-structures.<sup>9</sup> In fact, the extra diffraction spots in LEED for these orthorhombic  $\text{SrIrO}_3(001)$  films can be described as a  $(\sqrt{2}/4) \times (\sqrt{2}/4) \text{ R}45^\circ$  reciprocal space structure, as indicated by the extra diffraction spots in the LEED. Super-position of orthogonal rectangular lattice domains, also with a super periodicity, cannot be excluded either as the origin of the additional diffraction beams observed in the LEED (Figure 2b). Precise determination of the origin of the super-periodicity would be aided by intensity versus voltage analysis or the LEED or additional diffractions studies. Considering the cubic symmetry of the  $\text{SrTiO}_3$  substrate, such a super-periodicity can originate either from a surface reconstruction, or from lattice twinning of a rectangular distortion due to the collective rotation and tilt of the  $\text{Ir-O}_6$  octahedral,<sup>9</sup> at the subsurface layer.

To clarify which scenario can apply to our system, we combined the LEED data with the HR-ARPES results. Due to the large scattering cross-section of Ir, the penetration depth of LEED (31.5 eV electron energy) could be deeper than the photoemission mean free path at 150 eV: although very materials dependent, the electron mean free path frequently increases rapidly at kinetic energies below 50 eV, but rises only slowly at kinetic energies higher than 50 eV.<sup>25</sup> This is distinct from the LEED study shown in Ref. [9], which is performed at a much higher electron energy (120 eV) and thus more surface sensitive. Therefore, the fact that there is little evidence of band folding in the band structure, shown in Fig. 4, suggests that the topmost surface layer is not subject to a surface reconstruction at room temperature, and that the super periodicity arises well away from surface region. The explanation is that the angle-resolved photoemission is not influenced by multiple diffraction effects of the Sr-O top layer. Schütz et al.<sup>9</sup> attributes the  $\left(\sqrt{2}/2\right) \times \left(\sqrt{2}/2\right)$  R45° reciprocal space structure for insulating SrIrO<sub>3</sub> to a substrate clamping effect, which suppresses the Ir-O<sub>6</sub> octahedral distortions. Assuming similar clamping effect exists in our 5 nm (12.5 unit cell) films, the observed a  $\left(\sqrt{2}/4\right) \times \left(\sqrt{2}/4\right)$  R45° reciprocal space structure reveals a transition region from the interfacial layer (3 unit cell) to the topmost surface layer. The evolving crystal symmetry with distance from the substrate at this thickness range has previously been observed in epitaxial manganite thin films,<sup>28</sup> which has been attributed to competing misfit relaxation mechanisms. As orthorhombic SrIrO<sub>3</sub> is metastable in bulk, such dislocations/misfit can form due to the evolving lattice symmetry.<sup>10,29</sup> Another possible scenario is the heterogeneous placement of IrO<sub>6</sub> oxygen octahedra tilts across the 12 monolayers film, which can possess certain super-periodicity, although a super-periodicity near the surface near the surface appears excluded by the placement of the Brillouin zone edge in the band mapping. The lattice distortion can have pronounced impact on the electronic and magnetic properties of ultrathin SrIrO<sub>3</sub> films, and further affect the performance of SrIrO<sub>3</sub>-based electronic devices.<sup>29,30</sup>

## V. Conclusions

In conclusion, we have investigated the surface termination, electronic structure, crystal symmetry of strained orthorhombic SrIrO<sub>3</sub>(001) thin films on SrTiO<sub>3</sub> substrates. The Sr-O surface termination could contribute to the thickness-driven metal-insulator transition. While there is evidence in low energy electron diffraction of a super-periodicity, no band folding is seen in the experimental band structure, indicating an absence of surface reconstruction. The observed super-periodicity is attributed to a distortion of the orthorhombic structure well into the film, which may originate from the misfit relaxation from the epitaxial strain.

## Acknowledgement:

This work was supported by NSF through the Nebraska Materials Research Science and Engineering Center (MRSEC) Grant No. DMR-1420645 (structural, spectroscopy, and DFT studies), NSF Grant No. DMR-1710461 (sample growth and characterization), and Semiconductor Research Corporation (SRC) under GRC Task Number 2831.001 (modeling). The research was performed in part in the Nebraska Nanoscale Facility: National Nanotechnology Coordinated Infrastructure and the Nebraska Center for Materials and Nanoscience, which are supported by the National Science Foundation under Award ECCS: 1542182, and the Nebraska Research Initiative. The experiments have been performed under the approval of HiSOR (Proposal No. 18BG005 and 18BG006).



**Data Availability Statement:** The data that support the findings of this study are available from the corresponding author upon reasonable request.

## References

- <sup>1</sup>Q. Wang, Y. Cao, J. A. Waugh, S. R. Park, T. F. Qi, O. B. Korneta, G. Cao, and D. S. Dessau, *Phys. Rev. B* **87**, 245109 (2013).
- <sup>2</sup>D. Pincini, J. G. Vale, C. Donnerer, A. de la Torre, E. C. Hunter, R. Perry, M. Moretti Sala, F. Baumberger, and D. F. McMorrow, *Phys. Rev. B* **96**, 075162 (2017).
- <sup>3</sup>G. Chen and M. Hermele, *Phys. Rev. B* **86**, 235129 (2012).
- <sup>4</sup>B. J. Kim, H. Jin, S. J. Moon, J. Y. Kim, B. G. Park, C. S. Leem, J. Yu, T. W. Noh, C. Kim, S. J. Oh, J. H. Park, V. Durairaj, G. Cao, and E. Rotenberg, *Phys. Rev. Lett.* **101**, 076402 (2008).
- <sup>5</sup>S. J. Moon, H. Jin, K. W. Kim, W. S. Choi, Y. S. Lee, J. Yu, G. Cao, A. Sumi, H. Funakubo, C. Bernhard, and T. W. Noh, *Phys. Rev. Lett.* **101**, 226402 (2008).
- <sup>6</sup>T. Takayama, A. N. Yaresko, and H. Takagi, *J. Phys.: Condens. Matter* **31**, 074001 (2019).
- <sup>7</sup>Z. T. Liu, M. Y. Li, Q. F. Li, J. S. Liu, W. Li, H. F. Yang, Q. Yao, C. C. Fan, X. G. Wan, Z. Wang, and D. W. Shen, *Scientific Reports* **6**, 30309 (2016).
- <sup>8</sup>Y. F. Nie, P. D. C. King, C. H. Kim, M. Uchida, H. I. Wei, B. D. Faeth, J. P. Ruf, J. P. C. Ruff, L. Xie, X. Pan, C. J. Fennie, D. G. Schlom, and K. M. Shen, *Phys. Rev. Lett.* **114**, 016401 (2015).
- <sup>9</sup>P. Schütz, D. Di Sante, L. Dudy, J. Gabel, M. Stübinger, M. Kamp, Y. Huang, M. Capone, M. A. Husanu, V. N. Strocov, G. Sangiovanni, M. Sing, and R. Claessen, *Phys. Rev. Lett.* **119**, 256404 (2017).
- <sup>10</sup>L. Y. Zhang, B. Pang, Y. B. Chen, and Y. F. Chen, *Critical Reviews in Solid State and Materials Sciences* **43**, 367 (2018).
- <sup>11</sup>D. J. Groenendijk, C. Autieri, J. Girovsky, M. Carmen Martinez-Velarte, N. Manca, G. Mattoni, A. M. R. V. L. Monteiro, N. Gauquelin, J. Verbeeck, A. F. Otte, M. Gabay, S. Picozzi, and A. D. Caviglia, *Phys. Rev. Lett.* **119**, 256403 (2017).
- <sup>12</sup>J. Liu, D. Kriegner, L. Horak, D. Puggioni, C. Rayan Serrao, R. Chen, D. Yi, C. Frontera, V. Holy, A. Vishwanath, J. M. Rondinelli, X. Marti, and R. Ramesh, *Phys. Rev. B* **93**, 085118 (2016).
- <sup>13</sup>J. Longo, J. Kafalas, and R. Arnott, *J. Solid State Chem.* **3**, 174 (1971).
- <sup>14</sup>L. Zhang, Q. Liang, Y. Xiong, B. Zhang, L. Gao, H. Li, Y. B. Chen, J. Zhou, S.-T. Zhang, Z.-B. Gu, S.-h. Yao, Z. Wang, Y. Lin, and Y.-F. Chen, *Phys. Rev. B* **91**, 035110 (2015).
- <sup>15</sup>L. Zhang, X. Jiang, X. Xu, and X. Hong, e-print arXiv:1907.11814 (2019).
- <sup>16</sup>K. Shimada, M. Arita, Y. Takeda, H. Fujino, K. Kobayashi, T. Narimura, H. Namatame, and M. Taniguchi, *Surf. Rev. Lett.* **9**, 529 (2002).
- <sup>17</sup>H. Iwasawa, K. Shimada, E. F. Schwier, M. Zheng, Y. Kojima, H. Hayashi, J. Jiang, H. Higashiguchi, Y. Aiura, H. Namatame, and M. Taniguchi, *Synchrotron Radiation* **24** 836 (2017).
- <sup>18</sup>D. Vanderbilt, *Phys. Rev. B* **41**, 7892 (1990).
- <sup>19</sup>P. Giannozzi, et al., *J. Phys.: Condens. Matter* **21**, 395502 (2009).
- <sup>20</sup>J. P. Perdew, K. Burke, M. Ernzerhof, *Phys. Rev. Lett.* **77**, 3865 (1996).
- <sup>21</sup>P. V. C. Medeiros, S. Stafström, and J. Björk, *Phys. Rev. B* **89**, 041407(R) (2014).
- <sup>22</sup>P. V. C. Medeiros, S. S. Tsirkin, S. Stafström, and J. Björk, *Phys. Rev. B* **91**, 041116(R) (2015).
- <sup>23</sup>D. Briggs and M. P. Seah, *Practical Surface Analysis, Auger and X-Ray Photoelectron Spectroscopy* (Wiley, Chichester, 1996).
- <sup>24</sup>W. F. Egelhoff, *Surface Science Reports* **6**, 253 (1987).

This is the author's peer reviewed, accepted manuscript. However, the online version of record will be different from this version once it has been copyedited and typeset.

PLEASE CITE THIS ARTICLE AS DOI:10.1063/1.5135941

- <sup>25</sup>M. P. Seah and W. A. Dench, Surface and Interface Analysis **1**, 2 (1979).
- <sup>26</sup>G. Rijnders, D. H. A. Blank, J. Choi, and C.-B. Eom, Appl. Phys. Lett. **84**, 505 (2004)
- <sup>27</sup>H. Dulli, P. A. Dowben, S. -H. Liou, and E. W. Plummer, Phys. Rev. B **62**, R14629 (2000).
- <sup>28</sup>F. Sandiumenge, J. Santiso, L. Balcells, Z. Konstantinovic, J. Roqueta, A. Pomar, J. P. Espinos, and B. Martinez, Phys. Rev. Lett. **110**, 107206 (2013).
- <sup>29</sup>L. Zhang, X. G. Chen, H. J. Gardner, M. A. Koton, J. E. Shield, and X. Hong, Appl. Phys. Lett. **107**, 152906 (2015).
- <sup>30</sup>L. Zhang, H. J. Gardner, X. G. Chen, V. R. Singh, and X. Hong, J. Phys.: Condens. Matter **27**, 132201 (2015).

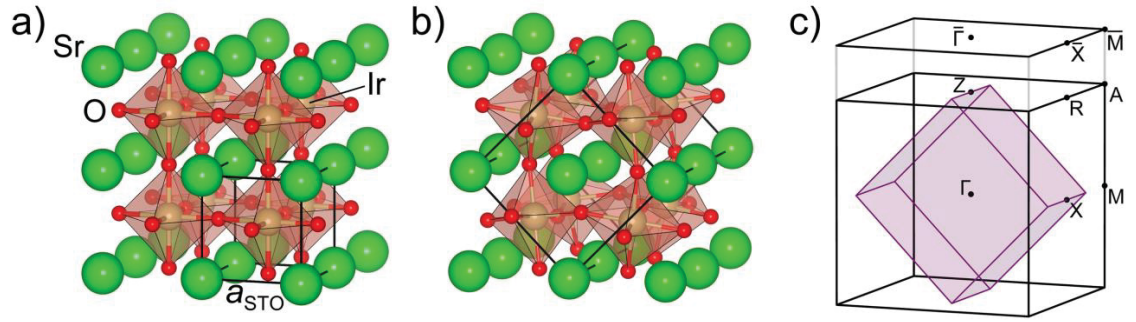


Figure 1. (a) The schematic of the crystal structure without distortion for SrIrO<sub>3</sub> epitaxially grown on the SrTiO<sub>3</sub> substrate. The black box denotes the ideal cubic perovskite unit cell. (b) The real crystal structure of SrIrO<sub>3</sub> with octahedral distortion. The black box denotes the orthorhombic unit cell, which is enlarged by  $\sqrt{2}a_0 \times 2a_0 \times \sqrt{2}a_0$  with respect to the unit cell shown in (a). (c) The Brillouin zone of orthorhombic SrIrO<sub>3</sub> (denoted by purple color), which can be unfolded into the large black Brillouin zone corresponding to the structure shown in (a). The surface Brillouin zone is shown in the top.



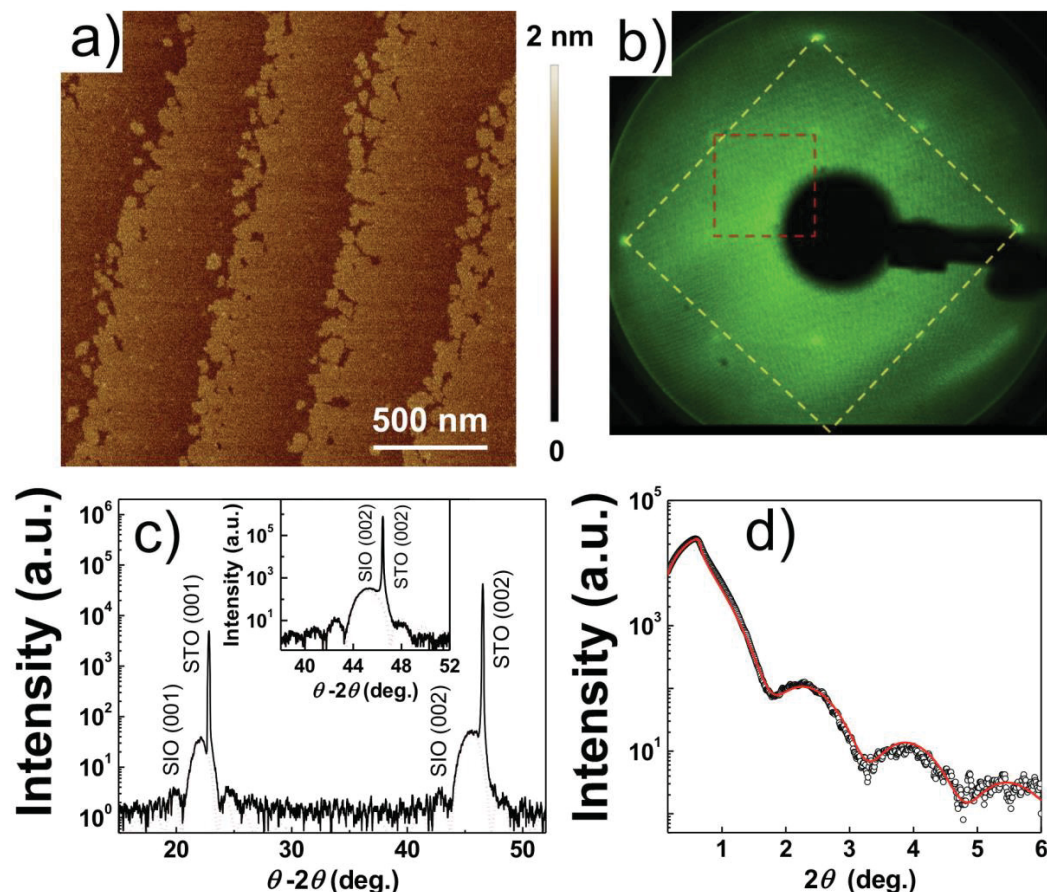


Figure 2. (a) the atomic force microscopy (AFM) image of a 5 nm orthorhombic  $\text{SrIrO}_3(001)$  film grown on  $\text{SrTiO}_3$  substrate showing atomically flat terraces. The RMS roughness of the film is  $\sim 2$  Å. (b) the corresponding low energy electron diffraction of 5 nm orthorhombic  $\text{SrIrO}_3(001)$  thin film grown on Nb doped  $\text{SrTiO}_3$  substrate. The electron energy is 31.5 eV. The yellow box highlights the reciprocal lattice of the integer order diffractions spots, while the red box highlights the faint diffractions spots due to the super periodicity. (c) X-ray diffraction  $2\theta$ - $\theta$  scan with fits to the Laue oscillations around the Bragg peaks of  $\text{SrIrO}_3$ . Inset: close-up scan around the (002) peak taken on another 5 nm film. Here  $\text{SrIrO}_3$  is denoted as SIO and  $\text{SrTiO}_3$  is denoted as STO. (d) The small angle X-ray diffraction (data in black) about the  $\text{SrIrO}_3(001)$  diffraction beam, with the fit to the data (red).

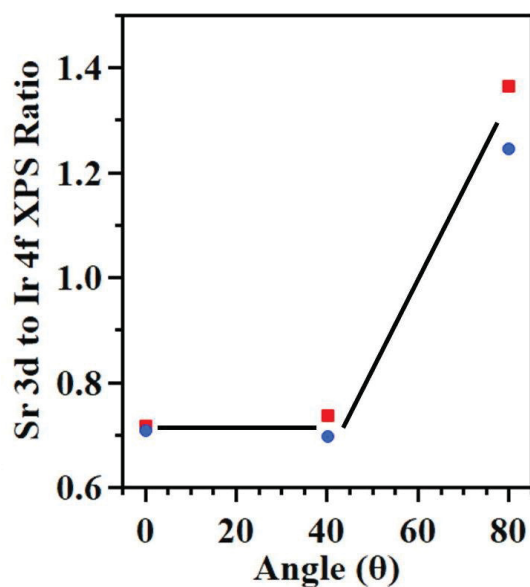


Figure 3. The Sr 3d core level to the combined Ir 4f and 5p<sub>1/2</sub> core levels photoemission intensities plotted as a function of angle. The emission angles are all with respect to the surface normal. Several successive sample annealing treatments, at ~150°C, changes the surface stoichiometry only slightly: red are the intensity ratios taken before and blue are taken after annealing.

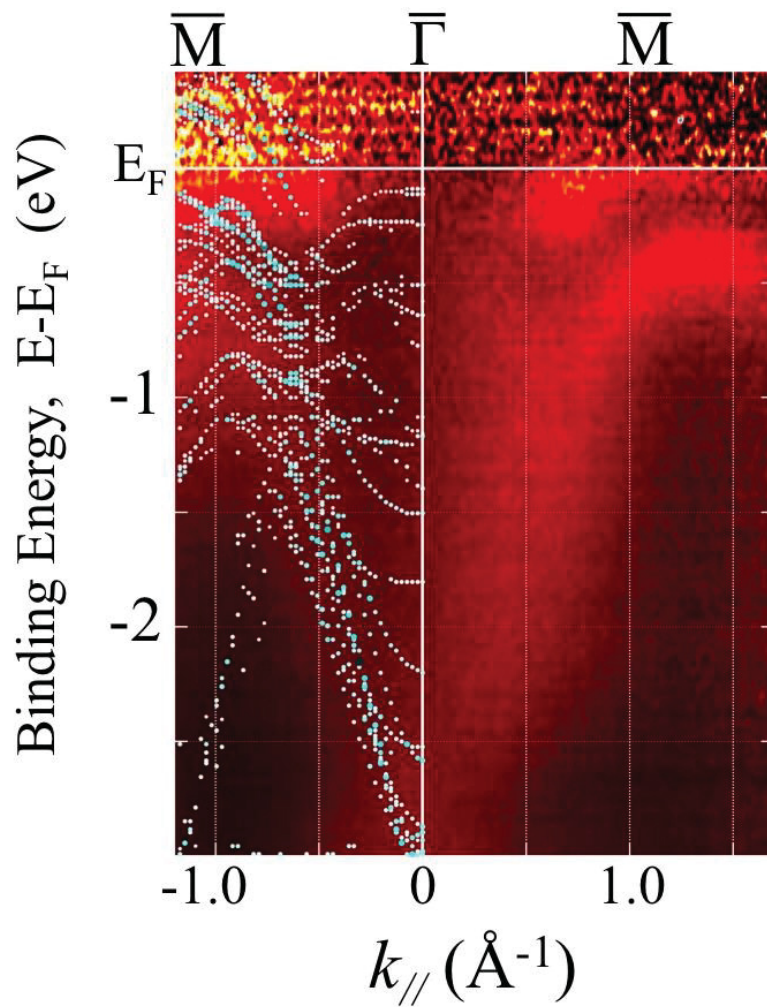


Figure 4. The experimental valence band electronic structure of a 5 nm thick orthorhombic  $\text{SrIrO}_3(001)$  thin films as derived from angle-resolved photoemission, taken at room temperature with a photon energy of 150 eV. Superimposed on experiment are the results from the DFT calculated band structure, on the left (light blue circles mark a large contribution to the spectral weight).